CZECH TECHNICAL UNIVERSITY IN PRAGUE

FACULTY OF MECHANICAL ENGINEERING

DOCTORAL THESIS STATEMENT

Czech Technical University in Prague
Faculty of Mechanical Engineering
Department of Mechanics, Biomechanics and Mechatronics

DOCTORAL THESIS STATEMENT

PHENOMENOLOGICAL MODELS FOR LIFETIME PREDICTION UNDER LOW-CYCLE FATIGUE AND THERMO-MECHANICAL FATIGUE LOADING CONDITIONS

by

Ing. Michal BARTOŠÁK

Doctoral Study Programme: Mechanical Engineering
Study Field: Mechanics of Rigid and Deformable Bodies and Environment

Supervisor: *Doc. Ing. Miroslav ŠPANIEL, CSc.*

Doctoral thesis statement for obtaining
the academic title of "Doctor" abbreviated to "Ph.D."

Prague, March 2019

Title: Phenomenological models for lifetime prediction under low-cycle fatigue and thermo-mechanical fatigue loading conditions

This doctoral thesis is an outcome of a full-time doctoral study programme at the Department of Mechanics, Biomechanics and Mechatronics, Faculty of Mechanical Engineering, Czech Technical University in Prague.

Disertant: Ing. Michal BARTOŠÁK
Department of Mechanics, Biomechanics and Mechatronics
Faculty of Mechanical Engineering
Czech Technical University in Prague
Technická 4, 166 07 Prague 6, Czech Republic
michal.bartosak@fs.cvut.cz

Supervisor: Doc. Ing. Miroslav ŠPANIEL, CSc.
Department of Mechanics, Biomechanics and Mechatronics
Faculty of Mechanical Engineering
Czech Technical University in Prague
Technická 4, 166 07 Prague 6, Czech Republic
miroslav.spaniel@fs.cvut.cz

Reviewers: _____

_____

_____

The thesis was set out on .....

The defense of the dissertation thesis will take place on .....

The thesis is available in the Department of Science and Research of Faculty of Mechanical Engineering, CTU in Prague, Technická 4, Praha 6 - Dejvice.

.....

prof. Ing. Michael Valášek, DrSc.
Head of Doctoral Study Field Mechanics of Rigid and Deformable Bodies and Environment
Faculty of Mechanical Engineering CTU in Prague

Title: Phenomenological models for lifetime prediction under low-cycle fatigue and thermo-mechanical fatigue loading conditions

Abstract:

This works presents original research data for low-cycle fatigue and thermo-mechanical fatigue of SiMo 4.06 cast iron. The cast iron was subjected to a various strain rates and strain amplitudes in the temperature range of 20°C-750°C under low-cycle fatigue and thermo-mechanical fatigue loading conditions. The experiments were carried out on the newly in-house designed test stand for performing uniaxial low-cycle and thermo-mechanical fatigue tests. A unified viscoplastic material is implemented by the means of user defined material subroutine for Abaqus commercial finite element software. The anisothermal multiaxial formulation of unified viscoplastic material model used here is based on hyperbolic sine flow rule and the model incorporates isotropic hardening and non-linear kinematic hardening. The model is calibrated systematically with temperature on the basis of obtained experimental data. A new method is applied in order to calibrate the temperature dependent viscoplastic material model parameters. Numerical simulations of cyclic mechanical behaviour of SiMo 4.06 follows. Finally, a novel energy based fatigue criterion is proposed in order to take into account effect of mean stress, which usually appears during thermo-mechanical loading. A good correlation was achieved between the predicted results and the observed results.

Keywords: viscoplasticity, thermo-mechanical fatigue, low-cycle fatigue, dissipated energy

Název: Fenomenologické modelování porušení se zaměřením na teplotní únavu

Anotace:

Tato disertační práce dokumentuje původní výsledky výzkumu nízkocyklové a teplotně-mechanické únavy tvárné litiny SiMo 4.06. Byly provedeny rozsáhlé mechanické zkoušky tohoto materiálu pro různé rychlosti a hladiny amplitud deformace, pro teploty v rozsahu 20°C-750°C. Mechanické zkoušky byly provedeny na nově navrženém zkušebním zařízení, které je určeno pro jednoosé zkoušky nízkocyklové a teplotně-mechanické únavy. Dále byl implementován unifikovaný viskoplastický materiálový model jako uživatelská funkce pro konečně-prvkový řešič Abaqus. Unifikovaný materiálový model je implementován pro případ multiaxiálního zatěžování za předpokladu proměnné teploty, konstitutivní vztah pro funkci tečení je založen na hyperbolickém sinu, model zahrnuje isotropní i nelineární kinematické zpevnění. Kalibrace modelu je provedena pro získané experimentální výsledky. Teplotně závislé parametry modelu jsou kalibrovány systematicky s využitím nových postupů. Zkalibrovaný materialový model je použit pro numerické simulace cyklického mechanického chování zkoumaného materiálu. Nakonec je navrženo nové kritérium pro hodnocení životnosti při nízkocyklové teplotně-mechanické únavě. Navržené kritérium je založeno na disipované hysterezní energii a zahrnuje vliv středního napětí, které je často pozorováno během mechanických zkoušek prováděných za proměnných teplot. Výsledky simulací dobře korelují s výsledky z experimentů.

Klíčová slova:

viskoplasticita, teplotně-mechanická únava, nízkocyklová únava, disipovaná energie

Contents

1 Introduction

Low-Cycle Fatigue (LCF) and Thermo-Mechanical Fatigue (TMF) are usually caused by the start-up and stop phases during the service life of a high-temperature component. In addition, long dwell periods, which can occur during service life, may lead to effects such as a creep and a stress relaxation that are both thermally dependent and activated processes. TMF and LCF are characterized by cyclic and time-dependent inelastic strains and stresses. If the temperature changes significantly during the loading cycle, TMF should be considered for life assessment, whereas LCF can be used for loading cycles with constant temperature. TMF is caused primarily by cyclic thermal loading and additional mechanical loading. The thermal loading is caused by inhomogeneous temperature fields and kinematic boundary conditions of the component that constrain thermal expansion and contraction and lead to inelastic time-dependent strains and stresses. In combination with additional mechanical loading, this result in component failure after several loading cycles. The TMF cycle is usually characterized by the phase between mechanical and thermal strain, primarily in-phase (IP-TMF), and out-of phase TMF tests (OP-TMF), Figs. 1a and 1b, respectively. High temperature LCF and TMF are important consideration in design phases of components in the course of variable service conditions, such as turbine housing of turbocharger, turbines, exhaust manifold, aircraft engine parts or fossil power-plant components. Reliable life prediction method is necessary in order to avoid over-dimensioning, and in order to guarantee functionality and safety of these components during their service life.

The classical LCF strain-life approach often is not a reliable method for TMF life predictions, since there are changes in temperature during the loading cycle. The mechanical response and the strain-life curves are temperature dependent. TMF can result in considerably shorter life in comparison with LCF for equivalent amplitude of loading and temperature. The reliable LCF/TMF life prediction method for complex components should consist from following parts:

- LCF and TMF experimental program for specimens,
- Constitutive material model derived from the material testing,
- Finite element analysis of the investigated component,
- Fatigue analysis of the component.

This work is structured as follows. First, current state of the problem is discussed in Chapter 2. Used methods are given in Chapter 3. Aims of the thesis are given in Chapter 4. The original experimental data are presented in

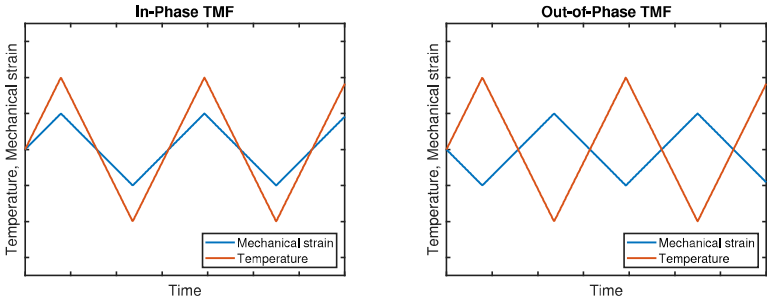

(a) (b)

Figure 1: In-phase (a) and out-of-phase (b) thermo-mechanical fatigue.

Chapter 5. In Chapter 6, a unified viscoplastic material model is chosen and is implemented as user material subroutine (UMAT) for Abaqus commercial finite element software. A novel method for systematic calibration of temperature dependent material model parameters is proposed. A novel fatigue criterion that is proposed on the basis of the observed lifetime behaviour of SiMo 4.06 is presented in Chapter 7. The criterion is based on the dissipated hysteresis energy, and is modified in order to take into account effect of changing temperature during the loading cycle. The outcomes of the thesis are described in Chapter 8. Finally, conclusions and possible topics for future research are given in Chapter 9.

2 State of the art

2.1 Experimental approaches to LCF and TMF

LCF and TMF loading conditions are usually simulated on specimens under strain control. Tabibian et al. [45] compared behaviour of lost foam cast aluminium alloys. Beck et al. [6] studied behaviour of Inconel under LCF and TMF loading. Sanicro 25 steel behaviour under OP-TMF and IP-TMF loading was studied by Petráš et al. [39]. Wu et al. [47] studied TMF behaviour of cast iron. Norman et al. [37] studied behaviour of three different types of silicon-molybdenum cast iron. Moreover, the experimental procedures for TMF were analysed in detail in [7, 17, 18].

2.2 Constitutive models used for LCF and TMF

The viscoplastic material models are capable of describing changes in the mechanical behaviour for wide temperature interval, and are often divided into two

groups. Non-unified viscoplastic material models [9, 15, 23, 31] treat creep strain and plastic strain separately [26]. In contrast, unified viscoplastic constitutive material models consider them in single quantity referred to as inelastic strain [8, 11, 12, 26, 29]. The unified material models are well suited for modelling viscoplastic behaviour under cyclic loading conditions. Whereas non-unified models leads to inaccurate ratcheting prediction and are not suited for cyclic loading conditions. In the framework of unified viscoplastic models, the viscoplastic strain rate is determined on the basis of chosen viscosity function. Chaboche [11, 12] used power-law function. Barrett et al. showed advantages of hyperbolic sine flow rule in [5].

Phenomenological viscoplastic material models are usually based on isotropic, kinematic hardening rules, associated flow rule and von Mises yield surface. Prager introduced linear kinematic hardening [40]. Non-linear kinematic hardening was proposed in [3]. Chaboche[10, 11, 26] used multiple backstress components to improve the prediction and also introduced the temperature term in the evolution law [11, 12]. Cyclic hardening or softening is taken into account in isotropic hardening function [12]. Furthermore, Chaboche introduced static recovery term in the kinematic hardening rule [11]. The unified Chaboche viscoplastic model and its modification have been used frequently. Kullig and Wipler [25] implemented isothermal version of this model with static recovery, where the effect of consistent tangent stiffness [43] on the speed of convergence was underlined. Consistent tangent stiffness for semi-implicit integration scheme of a unified viscoplastic model was studied in [4]. Constantinescu et al. [14] used two-layer viscoplasticity material model [24].

2.3 LCF and TMF life predictions methods

It is known that the oxidation, fatigue and creep are the main damage mechanisms involved in TMF and damage of each mechanism can be treated separately [35, 36, 41]. Total damage of the cycle, D_{total}, is then obtained as:

$$D_{total} = D_{oxidation} + D_{fatigue} + D_{creep}, \tag{1}$$

where $D_{oxidation}$ is oxidation damage, $D_{fatigue}$ is fatigue damage and D_{creep} is creep damage. Neu and Sehitoglu proposed calculation of individual damage mechanism in [35, 36, 41]. However, it requires considerable amount of material tests that are performed also in vacuum in order to separate oxidation damage. Therefore, it can be deduced that the damage model proposed by Neu and Sehitoglu is not well suited for engineering applications. This lead into that the oxidation effect is taken into account indirectly in most life prediction methods, because material tests are usually performed only under ambient conditions and

not in vacuum.

The classical strain-life approach is based on the work of Manson-Coffin, Ostergen and Smith-Watson-Topper [13, 19, 27, 38, 44]. Moreover, Palmgren-Miner linear damage accumulation is used in most cases. Well known Manson-Coffin fatigue criterion is written as: $\Delta\varepsilon_{pl} N_f^{\beta} = c$, where c and β are material parameters. $\Delta\varepsilon_{pl}$ is the plastic strain range of the loading cycle and N_f is number of cycles to failure. Halford and Manson [19] proposed strain range partitioning in order to treat creep and fatigue damage separately. Taira [46] proposed equivalent temperature of the loading cycle in order to take variable temperature during the loading cycle into account. Nagode et al.[32, 33] introduced Damage Operator Approach (DOA). This approach enables continuous fatigue and creep damage calculation during TMF loading. Nagode et al. used critical plane approach together with viscoplastic approximation in DOA in [34]. In the framework of energy based TMF and LCF prediction models, a key point is a hysteresis energy, w, which can be obtained by the numerical integration from the stabilized hysteresis loop as follows:

$$w = \int_{cycle} \boldsymbol{\sigma} : \dot{\boldsymbol{\varepsilon}}_m \, dt, \tag{2}$$

where $\boldsymbol{\sigma}$ is the stress tensor and $\dot{\boldsymbol{\varepsilon}}_m$ is the mechanical strain rate tensor. Constantinescu et al. used classical hysteresis energy criterion in [14]. This criterion was modified in [21]. Amiable et al. [1, 2] proposed modified hysteresis energy criterion with hydrostatic pressure term.

2.4 Discussion and conclusion

High temperature LCF and particularly TMF tests require expensive test stands with independent temperature and strain control. The unified viscoplastic models are usually not implemented or are implemented in basic version in commercial finite element software packages. Several implementations into FE software of such models were published, however consistent tangent stiffness (harder part) which is essential in order to solve large engineering problems, is mostly not published. Material parameters are usually calibrated for each temperature separately and then interpolated, this may lead to slow convergence for anisothermal loading. Hosseini et al. [22] proposed systematic calibration of the kinematic hardening parameters for a range of temperatures. The Sehitoglu and Neu TMF damage model requires large amount of tests, partly attained in vacuum, this requires expensive equipment. This damage model hardly fits industrial constraints. Therefore, several approaches were proposed, where the oxidation is taken into account indirectly. Nagode et al. proposed DOA. However, the viscoplastic approximation together with the critical plane approach

lead to long computational times. Several energy based LCF and TMF life prediction methods were proposed. The proposed criteria not always correctly reflected mean stress effect on the lifetime. The calculation of dissipated energy under multiaxial loading is more time efficient in comparison with the critical plane approach. Therefore, energy based criteria are possible subject of research.

3 Methods

3.1 The radial return algorithm

Implicit backward Euler (the radial return method) [16, 42] is used for numerical integration in Chapter 6. A basic principle is to compute a trial elastic stress increment, this yields new updated trial stress tensor, $\boldsymbol{\sigma}_{t+\Delta t}^{tr}$. Then, the stress tensor is updated with a plastic correction at time $t + \Delta t$. The subscript $_t$ denotes the value at the start of the increment. Hooke law can be written as [16, 42]:

$$\boldsymbol{\sigma} = \underbrace{2G\left(\boldsymbol{\varepsilon}_t^e + \Delta\boldsymbol{\varepsilon}\right) + \lambda Tr\left(\boldsymbol{\varepsilon}_t^e + \Delta\boldsymbol{\varepsilon}\right)\boldsymbol{I}}_{Elastic\ predictor} - \underbrace{2G\Delta\boldsymbol{\varepsilon}^{pl}}_{Plastic\ corrector} . \tag{3}$$

The stress tensor can be rewritten from Eq. 3 as a function of trial stress, i.e. elastic predictor, and effective plastic strain increment. Assuming multiaxial yield condition $f = \sigma_e - R - k = \sigma_e^{tr} - 3G\Delta p - R - k = 0$. This leads to a non-linear equation in Δp, that is usually solved by Newton iterative method. Finally, after obtaining effective plastic strain increment, the elastic strain tensor increment is obtained so that stress tensor increment is obtained on the basis of Hooke law.

3.2 Minimum of constrained non-linear multi-variable function

Function *Find a minimum of constrained non-linear multi-variable function* from Matlab [28] is used in order to optimize values of kinematic hardening parameters with temperature in Chapter 6.

3.3 Non-linear least square method

Non-linear least-squares solver available in MATLAB [28] is used for calibration of fatigue criteria and the material model parameters. Lower and upper bounds are used here, therefore the trust-region-reflective algorithm [28, 30] is applied.

3.4 Prediction bounds

The prediction bounds are used in Chapter 7 to measure the confidence that the new observation lies in the interval given by a single predictor value $y \pm t_{1-\alpha/2} s \sqrt{1 + x \left(X^T X\right)^{-1} x^T}$, where s is the standard error, $t_{1-\alpha/2}$ denotes the inverse of Student cumulative distribution. X is the design vector of explanatory variables. y is the fitted or predicted value of predictor x [20].

4 Aims of the thesis

Aims of the thesis were chosen on the basis of conclusions defined in the Chapter 2. The aims can be summarized into the following points:

1. Proposal of a novel energy based fatigue criterion that can be used for lifetime predictions under LCF and TMF loading. Main requirements for the criterion are that it is robust and usable for lifetime predictions of complex engineering structures.
2. Development of the control algorithms for the newly in-house designed test stand, which was designed with a view of cost-effectiveness, and that can be used for uniaxial strain controlled LCF and TMF tests.
3. Experimental research of SiMo 4.06 mechanical behaviour under TMF and LCF loading conditions. Acquirement of new experimental data in order to calibrate a viscoplastic material model and a novel fatigue criterion.
4. Implementation and numerical integration of the selected unified viscoplastic material model as UMAT for Abaqus. Formulation, derivation and validation of consistent tangent stiffness that is a key point for solving large engineering problems.
5. Development of the calibration tool for the material model. Proposal of a novel method for calibration of temperature dependent material parameters. Validation of the calibrated material model.

5 Experiments

5.1 A new test stand

The material tests were carried out on an in-house designed test stand [A.1, A.9, A.11, A.12, A.13, A.16], Fig. 2a. The test stand was designed as a jig to an Instron servo-hydraulic actuator. The specimen is heated by direct electrical

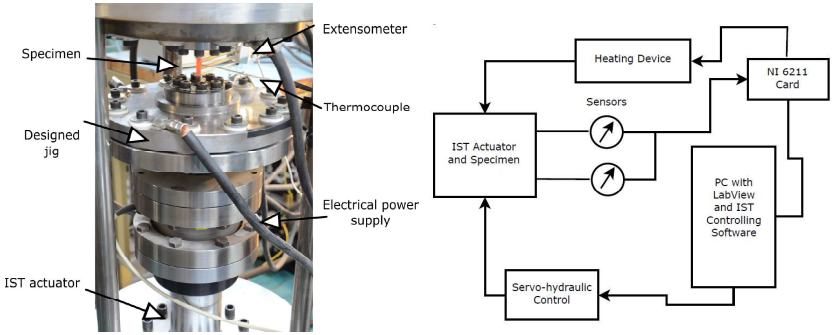

(a) (b)

Figure 2: Test stand for LCF/TMF testing (a) and closed-loop control of the LCF/TMF test stand (b).

resistance heating. The temperature is measured by the thermocouple in the center of the specimen. The strain is controlled by the high temperature extensometer. The force is measured by the built-in load cell. The PC based system is connected with a NI-DAQ measurement card that collects the data from the sensors. Closed-loop control is presented in Fig. 2b.

5.2 Investigated material

The material under investigation is silicon molybdenum (SiMo) cast iron with a spherical graphite, annealed. Good cast-ability and relatively low price makes SiMo a good and popular choice in the automotive industry, where it is used in the production of turbine housings and exhaust manifolds.

5.3 Test conditions

Strain-controlled LCF and TMF tests were performed under ambient conditions for cylindrical specimens. The LCF tests were performed with and without a dwell time between 20°C and 750°C, fully reversed, for variable mechanical strain ranges $\Delta\varepsilon_m$ from 0.005 to 0.025. The LCF tests with 300 s hold time in tension were carried out for $\Delta\varepsilon_m$= 0.012. The LCF tests were performed with a constant mechanical strain rate, $\dot{\varepsilon}_m = 0.003\ s^{-1}$. The TMF tests were performed as out-of-phase tests (OP-TMF) with a minimum test temperature of 100°C and with a maximum test temperature of 650°C. The thermal strain was totally suppressed for the tests, so the total strain was kept constant. The heating phase lasted 104 s, followed by cooling in air, 240 s total time [A.1, A.9, A.11, A.12, A.14, A.15].

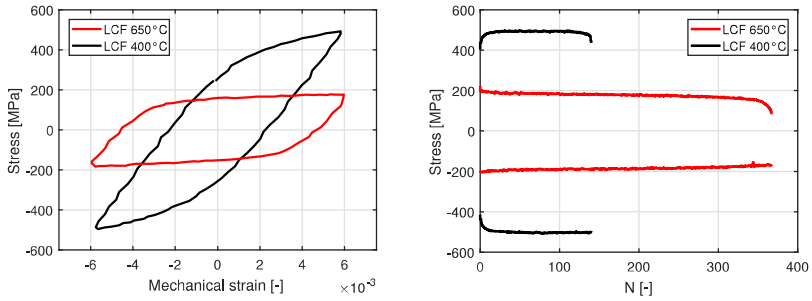

(a) (b)

Figure 3: Stabilized hysteresis loops (a) and maximum and minimum stress as a function of the number of cycles for the LCF tests (b).

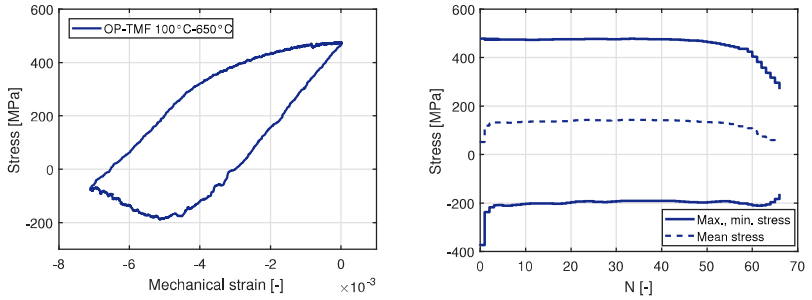

(a) (b)

Figure 4: Stabilized hysteresis loop for the OP-TMF test (a) and maximum, minimum and mean stress as a function of the number of cycles for the OP-TMF test (b).

5.4 New experimental results

The cyclic mechanical behaviour [A.1, A.3, A.9, A.15] of SiMo is presented in Figs. 3a-4b for LCF tests and OP-TMF test, respectively. Fig. 5a [A.1] presents the results of the LCF tests with 300 s hold time in tension in the form of the evolution of the relaxed part of the stress in comparison with the total stress with temperature. The relaxed part of the stress corresponds to the viscous part of the stress. Fig. 5b presents data obtained for the LCF test with 300 s hold time in tension at 500°C [A.1]. The LCF results and TMF results are also presented in Chapter 6 and 7.

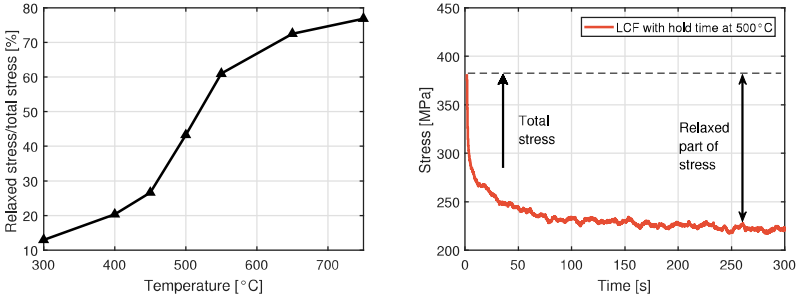

(a) (b)

Figure 5: Evolution of the relaxed stress compared to the total stress with temperature in the LCF tests with a hold time in tension(a) and cyclic relaxation test at 500°C (b).

5.5 Discussion and conclusion

The in-house designed LCF/TMF test stand [A.1, A.9], [A.11]- [A.16] presented here can be used for performing uniaxial TMF/LCF tests on cylindrical and notched specimens under passive cooling under ambient air. The proposed design is significantly less expensive than commercial LCF/TMF test stands. SiMo 4.06 showed cyclic hardening below 500°C and cyclic softening above 500°C under LCF loading. The cylindrical specimens showed increasing durability in the high strain ranges with increasing test temperature. However, the durability for the low strain range tests decreased with increasing test temperature. The investigated material undergoes strong time-dependent effects with increasing temperature, as is observed in the relaxation tests. The OP-TMF test results for cylindrical specimens demonstrate the negative effect of positive mean stress on the lifetime of SiMo 4.06. The lifetime is significantly reduced in comparison with the LCF test results.

6 A unified viscoplastic material model

6.1 Viscoplastic constitutive material model

The mechanical strain rate tensor, $\dot{\boldsymbol{\varepsilon}}$, can be decomposed into the elastic part, $\dot{\boldsymbol{\varepsilon}}^{\boldsymbol{e}}$, and into the inelastic part, $\dot{\boldsymbol{\varepsilon}}^{\boldsymbol{pl}}$, as $\dot{\boldsymbol{\varepsilon}} = \dot{\boldsymbol{\varepsilon}}^{\boldsymbol{e}} + \dot{\boldsymbol{\varepsilon}}^{\boldsymbol{pl}}$. The stress rate tensor is obtained on the basis of the generalized Hooke law as:

$$\dot{\boldsymbol{\sigma}} = \boldsymbol{E} : \dot{\boldsymbol{\varepsilon}}^{\boldsymbol{e}}, \tag{4}$$

where $\boldsymbol{E}$ is the fourth order elasticity tensor. The dissipation potential [26], denoted as Ω, Fig. 6, is used to obtain the effective viscoplastic strain rate, $\dot{p}$, in Eq. 5 and the inelastic strain tensor rate in Eq. 6.

$$\dot{p} = \frac{\partial \Omega}{\partial f} = \alpha \sinh\left(\beta f\right), \tag{5}$$

$$\dot{\boldsymbol{\varepsilon}}^{\boldsymbol{pl}} = \frac{\partial \Omega}{\partial \boldsymbol{\sigma}} = \frac{\partial \Omega}{\partial f}\frac{\partial f}{\partial \boldsymbol{\sigma}} = \dot{p}\boldsymbol{n} = \frac{3}{2}\dot{p}\frac{\boldsymbol{s} - \boldsymbol{x_D}}{J\left(\boldsymbol{\sigma} - \boldsymbol{x}\right)}, \tag{6}$$

where α and β are temperature and material dependent model parameters. $\boldsymbol{s}$ is the stress tensor deviator, and $\boldsymbol{n}$ is the tensor normal. $\boldsymbol{x}$ is the kinematic hardening tensor, and $\boldsymbol{x_D}$ is its deviator, also $\boldsymbol{x} = \boldsymbol{x_D}$. The stress function, f, is defined as $f\left(\boldsymbol{\sigma} - \boldsymbol{x}\right) = J\left(\boldsymbol{\sigma} - \boldsymbol{x}\right) - k - R$, where k is the initial yield stress and R denotes the isotropic hardening function. $f \leqslant 0$ defines the elastic domain, whereas for $f \geq 0$ the behaviour is viscoplastic and $\dot{p}$ is determined by the selected flow rule. $J\left(\boldsymbol{\sigma} - \boldsymbol{x}\right)$ is the von Mises invariant.

The non-linear kinematic hardening model rule proposed by Chaboche [10, 11] states that the overall backstress is composed of multiple components, $\boldsymbol{x} = \sum_{i=1}^{N} \boldsymbol{x}_i$. The non-isothermal evolution law of the backstress component is defined as:

$$\dot{\boldsymbol{x_i}} = \frac{2}{3}C_i\dot{\boldsymbol{\varepsilon}}^{\boldsymbol{pl}} - \gamma_i \boldsymbol{x_i}\dot{p} + \frac{1}{C_i}\frac{\partial C_i}{\partial T}\boldsymbol{x_i}\dot{T} \tag{7}$$

where C_i and γ_i are temperature-dependent and material-dependent parameters. The isotropic hardening evolution used here is defined in a classical way as follows:

$$\dot{R} = b\left(Q - R\right)\dot{p} + \left(\frac{1}{b}\frac{\partial b}{\partial T} + \frac{1}{Q}\frac{\partial Q}{\partial T}\right)R\dot{T}, \tag{8}$$

where b and Q are temperature and material dependent parameters.

6.2 FEM implementation of viscoplastic material model

Numerical integration of constitutive equations

The implicit integration scheme, Chapter 3, is used in this work [A.3, A.5]. Then, the effective viscoplastic strain increment is obtained on the basis of the constitutive equations as follows:

$$\dot{p} = \frac{\Delta p}{\Delta t} = \phi\left(\Delta p, \boldsymbol{x}, R\right) = \alpha \sinh \beta\left(\sigma_e^{tr} - 3G\Delta p - R - k\right) \tag{9}$$

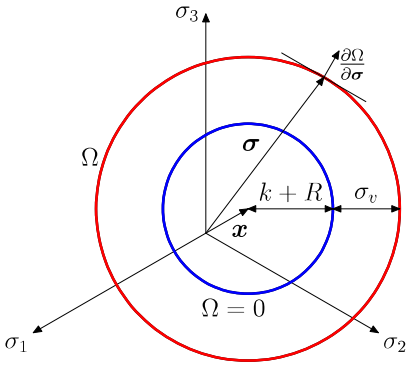

Figure 6: The elastic domain ($\Omega = 0$) and the viscoplastic domain (Ω) in 3D stress space.

Eq. 9 can be rewritten in the incremental form that can be employed for the Newton iterative method, which is used to obtain the increment in the effective viscoplastic strain Δp:

$$\varphi = \Delta p - \phi\left(\Delta p, \boldsymbol{x}, R\right)\Delta t = 0 \tag{10}$$

Eq. 10 is a non-linear equation, which can be solved by the Newton iterative method. After rearrangement and substitution, the iterative form is obtained as follows [5]:

$$d\Delta p = \frac{\phi - (\Delta p/\Delta t) - Z\boldsymbol{n} : \boldsymbol{x_i}\dfrac{1}{C_i}\dfrac{\partial C_i}{\partial T}\Delta T - Z\left(\dfrac{1}{b}\dfrac{\partial b}{\partial T} + \dfrac{1}{Q}\dfrac{\partial Q}{\partial T}\right)RdT}{\dfrac{1}{\Delta t} + 3GZ + ZC_i - Z\boldsymbol{n} : \boldsymbol{x_i}\gamma_i + Zb\left(Q - R\right)} \tag{11}$$

The increment in the effective viscoplastic strain, $\Delta p = \Delta p + d\Delta p$, is updated until convergence is obtained. Moreover, when the increment in the effective viscoplastic strain, Δp, is obtained, the increment in the plastic strain tensor, $\Delta\boldsymbol{\varepsilon}^{pl}$, can be obtained on the basis of Eq. 6. Finally, the stress increment is obtained on the basis of the generalized Hooke law.

Consistent material tangent operator

In this study, the consistent material tangent operator is analytically derived on the basis of the implicit integration scheme that is used [A.3, A.5]. The first

point in the derivation of the consistent material tangent operator is the stress tensor normal:

$$\frac{3}{2}\frac{\boldsymbol{s}-\boldsymbol{x_D}}{\sigma_e} = \frac{3}{2}\frac{\boldsymbol{s^{tr}}-\boldsymbol{x_D}}{\sigma_e^{tr}} \tag{12}$$

Rearranging, applying the differential operator and substituting of Eq. 12 gives the following form:

$$\begin{gathered}\delta\sigma = K\boldsymbol{II}:\delta\boldsymbol{\varepsilon} + \frac{\sigma_e}{\sigma_e^{tr}}\left(2G\delta\boldsymbol{\varepsilon} - \frac{2}{3}G\boldsymbol{II}:\delta\boldsymbol{\varepsilon}\right) + \left(1-\frac{\sigma_e}{\sigma_e^{tr}}\right) \\ \left(\frac{2}{3}C_i\delta\Delta p\boldsymbol{n} - \gamma_i\boldsymbol{x_i}\delta\Delta p + \frac{1}{C_i}\frac{\partial C_i}{\partial T}\boldsymbol{x_i}\Delta T\right) + \frac{\boldsymbol{s^{tr}}-\boldsymbol{x}}{\sigma_e^{tr}}\left(\delta\sigma_e - \frac{\sigma_e}{\sigma_e^{tr}}\delta\sigma_e^{tr}\right)\end{gathered} \tag{13}$$

At this point, $\delta\Delta p$ in Eq. 13 should be derived from the integration scheme. Substituting final form of $\delta\Delta p$ into Eq. 13 and rearranging gives [A.3, A.5]:

$$\begin{gathered}\delta\boldsymbol{\sigma} = Z_1\delta\boldsymbol{\varepsilon} + Z_2\boldsymbol{II}:\delta\boldsymbol{\varepsilon} + \boldsymbol{n}Z_3\boldsymbol{n}\delta\boldsymbol{\varepsilon} + \boldsymbol{n}\left(\boldsymbol{n}:I\right)Z_4\boldsymbol{I}:\boldsymbol{\varepsilon} - \boldsymbol{x}_iZ_{5i}\boldsymbol{n}:\boldsymbol{\varepsilon} + \\ \boldsymbol{x}_iZ_{6i}\left(\boldsymbol{n}:\boldsymbol{I}\right):\delta\boldsymbol{\varepsilon} + \left(\boldsymbol{s^{tr}}-\boldsymbol{x}\right)Z_7\boldsymbol{n}:\delta\boldsymbol{\varepsilon} - \left(\boldsymbol{s^{tr}}-\boldsymbol{x}\right)Z_8\left(\boldsymbol{n}:\boldsymbol{I}\right)\boldsymbol{I}:\delta\boldsymbol{\varepsilon} + \\ \left(1-\frac{\sigma_e}{\sigma_e^{tr}}\right)\left[\frac{H}{D}\left(\frac{2}{3}C_i\boldsymbol{n}-\gamma_i\boldsymbol{x}_i\right) + \frac{1}{C_i}\frac{\partial C_i}{\partial T}\boldsymbol{x}_i\Delta T\right] + \\ \frac{\boldsymbol{s^{tr}}-\boldsymbol{x}}{\sigma_e^{tr}}\left[\frac{H}{D}\left(1-\frac{\sigma_e}{\sigma_e^{tr}}\right)\left(C_i-\gamma_i\boldsymbol{n}:\boldsymbol{x}_i\right) + \frac{H}{D}3G - \left(1-\frac{\sigma_e}{\sigma_e^{tr}}\right)\frac{1}{C_i}\frac{\partial C_i}{\partial T}\boldsymbol{n}:\boldsymbol{x}_i\Delta T\right]\end{gathered} \tag{14}$$

The terms used in Eq. 14, $Z_1 - Z_7$ and H/D, are given in [A.3, A.5]. Finally, the Jacobian matrix is obtained as $\boldsymbol{J} = \dfrac{\partial\delta\boldsymbol{\sigma}}{\partial\delta\boldsymbol{\varepsilon}}$.

6.3 A novel calibration of viscoplastic material model

In this section, the implemented material model is calibrated from the obtained experimental data [A.1, A.3, A.5, A.9, A.11, A.14, A.15]. Then the model is used for a numerical description of the cyclic mechanical behaviour of the studied material using FEM. The first step is to calibrate the elastic modulus. The next step is to determine the kinematic hardening properties that are calibrated on the basis of stabilized state at mid-life. The tensile part of the corresponding hysteresis curve can therefore be written as follows:

$$\sigma = k'' + \frac{C_1}{\gamma_1}\left(1-2\exp\left(-\gamma_1\varepsilon_{pl}\right)\right) + \frac{C_2}{\gamma_2}\left(1-2\exp\left(-\gamma_2\varepsilon_{pl}\right)\right) + C_3, \varepsilon_{pl} \tag{15}$$

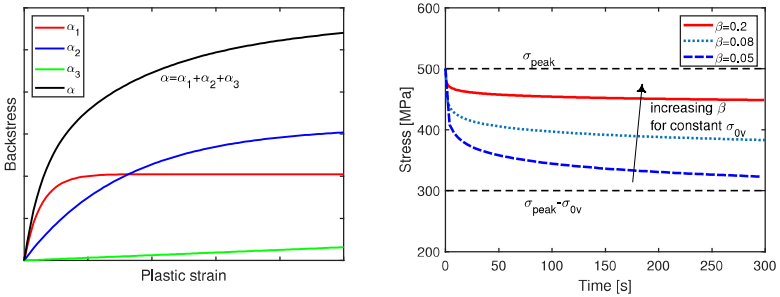

(a) (b)

Figure 7: The additive superposition of individual backstress components (a) and the variation of viscous parameter β for a constant relaxed stress value (b).

where ε_{pl} is the uniaxial inelastic strain. k'' is the yield stress that meanwhile also incorporates the viscous part of the stress. Temperature dependent non-linear kinematic hardening parameters were calibrated to follow a monotonic downward trend at temperature described mathematically as the Boltzmann function [A.2, A.3, A.4, A.5, A.7, A.8, A.10, A.11, A.14, A.15]:

$$C_{1-3}(T) = \frac{a_{01-03} - a_{04-06}}{1 + \exp(\frac{T - a_{07}}{a_{08}})} + a_{04-06},\ \gamma_{1-2}(T) = \frac{b_{01-02} - b_{03-04}}{1 + \exp(\frac{T - b_{05}}{b_{06}})} + b_{03-04} \quad (16)$$

where a_{01-08} and b_{01-06} are the calibrated parameters. γ_3 is considered to be zero. In the calibration process, five stabilized hysteresis loops for different temperatures at mid-life were selected from the isothermal LCF tests. The principle was to search the global minimum of the objective function, which was defined as the sum of squares of the percentage differences between the tested and the simulated stress. A general rule for kinematic hardening parameters was used in the process for calibrating the kinematic hardening parameters Fig. 7a.

The next step is to determine the temperature-dependent viscous parameters from the isothermal LCF tests with the hold time in tension. The stress as a function of time during the strain hold period can be written as:

$$\sigma(t) = x + R + k + \frac{2}{\beta} \tanh^{-1}\left(\tanh\left(\frac{\beta\left(\sigma_{peak} - x - R - k\right)}{2}\right) e^{-\alpha\beta E t}\right), \quad (17)$$

where σ_{peak} is the maximum stress value. Moreover, the value of $\sigma_{peak} - \sigma_{0v}$ is equal to $x + R + k$ [A.3, A.5]. After rearranging, the calibrated parameters are the viscous part of the stress σ_{0v} and β. They are obtained by the non-linear least square method from the experimental data. The variation of β is presented

in Fig. 7b for constant value of initial overstress σ_{0v}. The initial value of yield stress k'' should be corrected after the parameters controlling viscous behaviour have been estimated. The last step in the calibration process is to determine the isotropic hardening properties, Q and b. The evolution of isotropic hardening function R with accumulated inelastic strain p can be derived explicitly from Eq. 8 for the isothermal case $R(p) = Q\left(1 - e^{-bp}\right)$. The final yield stress value k must be calibrated together with b and Q.

6.4 Results

Cyclic mechanical behaviour of SiMo 4.06

The constitutive material model parameters were estimated by a step-by-step procedure [A.3, A.5]. The simulated and experimental hysteresis loops for mechanical strain rate $\dot{\varepsilon} = 0.003\ s^{-1}$ at 20°C in 100th cycle and at 650°C for the 200th cycle are presented in Figs. 8a and 8b, respectively. The hysteresis loops for the LCF tests with hold time in tension [A.3] are presented in Figs. 10a and 11a for 400°C and 550°C, respectively. The stress relaxation during the hold period is presented in Figs. 10b and 11b for 400°C and 550°C, respectively. The results at 650°C for mechanical strain rates 0.00001 s^{-1} and 0.0003 s^{-1} are showed in Figs. 12a and 12b. Next, the unified viscoplastic constitutive material model is used to simulate the mechanical response of the SiMo 4.06 under OP-TMF loading. The temperature and the mechanical strain loading history are presented in Fig. 13a. It can be observed that the strain rate was variable during the loading cycle. The observed hysteresis loop and the simulated hysteresis loop for the 30th cycle are presented in Fig. 13b for the OP-TMF test [A.1, A.9, A.14, A.15]. In conclusion, the used hyperbolic sine flow rule results in good prediction of viscous stress, which can be observed in the form of relaxation or strain-rate sensitivity [A.3, A.5].

Validation of consistent tangent stiffness

A notched cylindrical specimen, Fig. 14, is chosen as a numerical example in order to study the performance and the speed of convergence of the derived Consistent Tangent Stiffness (CTS) in Abaqus commercial finite element software [A.3, A.5]. The symmetry boundary condition is applied to the bottom of the specimen, and the displacement boundary condition, $u_y = 0.05$, is applied on the top. The temperature is set equal to 450°C, and the length of the loading step is 25 s. First, the speed of convergence of the CTS is compared with the computations with elastic stiffness. The convergence criterion for the largest residual force of the global Newton method is set to the default value

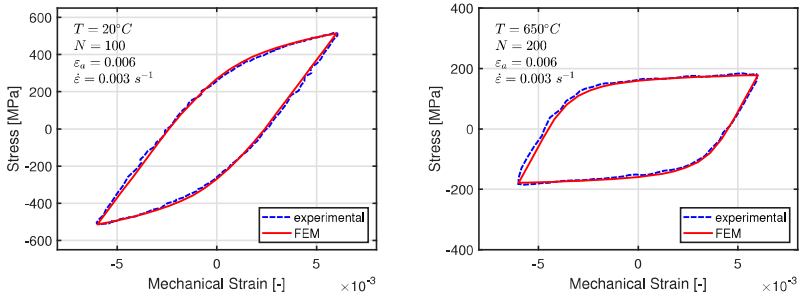

(a) (b)

Figure 8: LCF response for strain rate 0.003 s^{-1}, hysteresis loop for the 100th cycle at 20°C (a) and for the 200th cycle at 650°C (b).

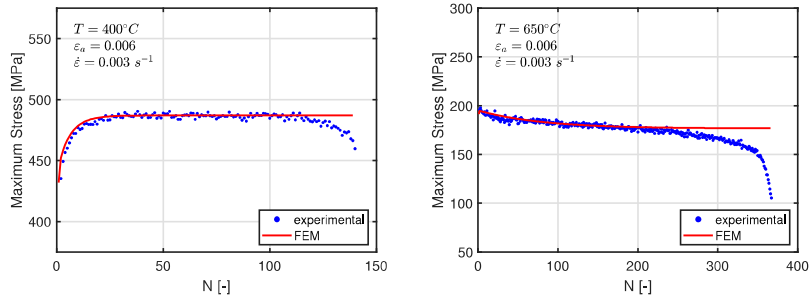

(a) (b)

Figure 9: Cyclic evolution of the maximum stress during triangular LCF tests at 400°C (a) and at 650°C (b) for strain rate 0.003 s^{-1}.

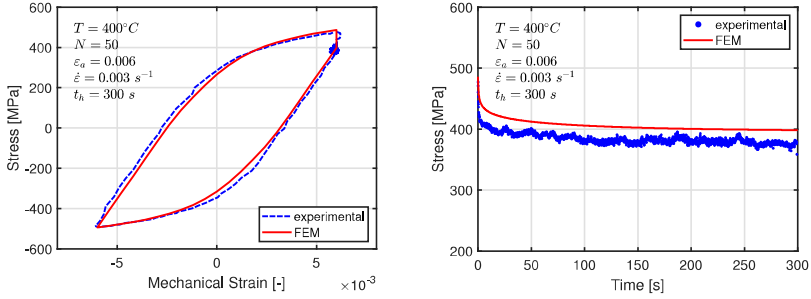

(a) (b)

Figure 10: LCF with 300 s hold time at 400°C, hysteresis loop for the 50th cycle (a) and corresponding stress relaxation during the hold time (b).

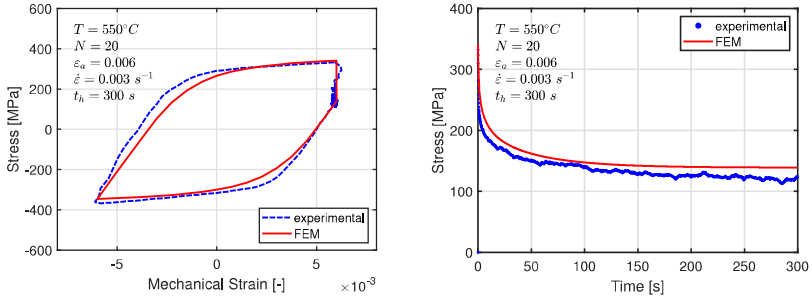

(a) (b)

Figure 11: LCF with 300 s hold time at 550°C, hysteresis loop for the 20th cycle (a) and the corresponding stress relaxation during the hold time (b).

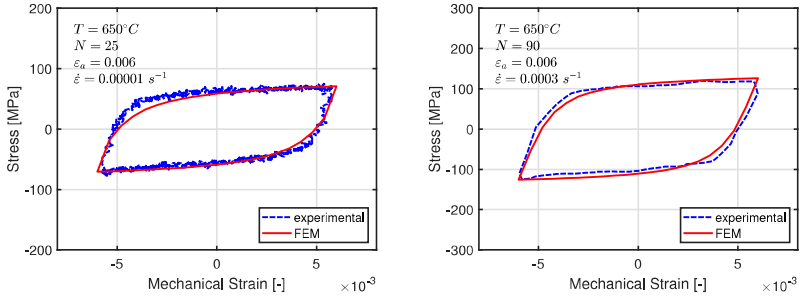

(a) (b)

Figure 12: LCF response at 650°C, hysteresis loop for the 25th cycle for strain rate 0.00001 s^{-1} (a) and the hysteresis loop for the 90th cycle for strain rate 0.0003 s^{-1} (b).

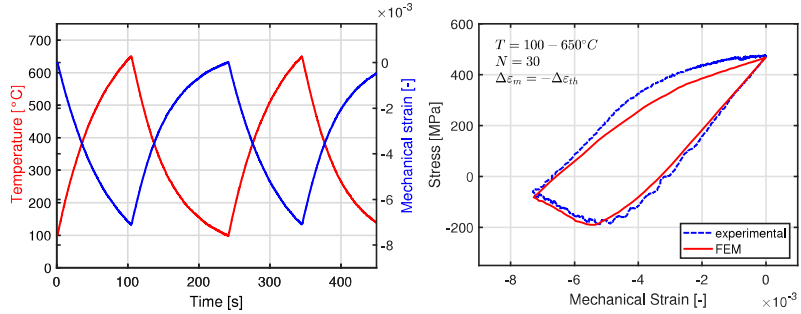

(a) (b)

Figure 13: OP-TMF response between 100°C and 650°C, temperature and mechanical strain history during the OP-TMF test (a) and the hysteresis loop for the 30th cycle (b).

in Abaqus, which is equal to $5.10^{-3}N$. The results of this study are presented in Tab.1. The consistent tangent stiffness needed only one increment to complete the step. If we compare the total number of equilibrium iterations, we can observe a much lower numerical cost for consistent tangent stiffness than for elastic stiffness. Next, the convergence criterion for the largest residual force of the global Newton method is set to $5.10^{-7}N$ in order to study the speed of convergence for consistent tangent stiffness. The results in terms of the largest residual force for each iteration are presented in Tab.2, where the results show quadratic convergence of the global Newton method.

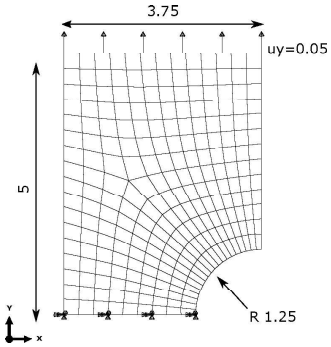

Figure 14: Finite element model of a notched cylindrical specimen.

7 A novel fatigue criterion

7.1 Investigation of dissipated energy per cycle

The dissipated energy per cycle, w, is obtained on the basis of Eq. 2 from the experimental data at mid-life, and is plotted versus the number of cycles to failure, N_f, in Fig. 15 [A.1], where R^2LCF denotes the coefficient of determination and is computed from the experimental triangular LCF data obtained for all tested temperatures and the regression line. End-life was determined when a 5% drop in peak stress occurred in comparison with the stabilized state. The regression

Table 1: Number of increments (NI) and total equilibrium iterations (NEI).

	NI	NEI
CTS	1	9
Elastic stiffness	16	77

results, described here by the coefficient of determination $R^2LCF = 0.875$, confirm that temperature has no major influence on the dependency between the dissipated energy per cycle and the number of cycles to failure. Therefore, the LCF data, in terms of the dissipated energy and the lifetime, do not additionally have to be splitted by temperature [A.1]. OP-TMF data are added in Fig. 15 to illustrate the shorter lifetime of these specimens in comparison with the LCF results. This difference is also caused by the influence of the positive mean stress for the OP-TMF. For the LCF tests, the mean stress is close to zero.

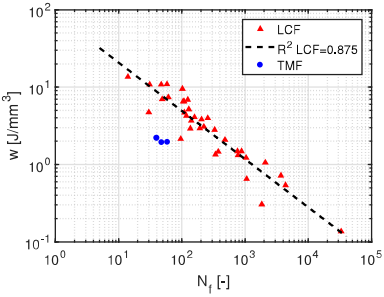

Figure 15: Dissipated energy per cycle versus the number of cycles to failure.

The specimens showed monotonically increasing durability in high strain ranges with increasing temperature. A decrease in lifetime was observed with increasing temperatures for low strain range tests [A.1, A.2, A.9]. In terms of the dissipated energy per cycle versus the number of cycles to failure, no significant difference is observed [A.1].

7.2 A novel fatigue criterion

In this work, a energy-based criterion is proposed for predicting LCF and TMF [A.1]. The LCF results presented here show that temperature has no major influence on the dependency between the dissipated energy per cycle and the number of cycles to failure for SiMo, Fig. 15. Therefore, no temperature term is included in the proposed criterion [A.1]. The oxidation effect is taken into ac-

Table 2: Values of the largest residual force in equilibrium iterations for the selected increment.

Equilibrium iteration	1	2	3	4
Largest residual force [N]	2.88	1.08E-02	2.31E-05	5.30E-08

count indirectly, as the material tests were performed under ambient conditions [A.1]. The mean stress effect is taken into account by means of the modified dissipated energy per cycle, $\widetilde{w}$, as follows:

$$\widetilde{w} = AN_f^B, \tag{18}$$

where A and B are the material parameters obtained by the least squares method from the LCF test data from all temperatures, and correspond to the regression line in Fig. 15. The effect of mean stress on lifetime for the OP-TMF test is considerable for SiMo. The modified dissipated energy per cycle $\widetilde{w}$ is suggested, including the mean stress term, as follows:

$$\widetilde{w} = w + \alpha(-1 - R_\sigma^{-1}), \tag{19}$$

where α is an additional material parameter, which is obtained by the least squares method from the TMF test results, and w is the cycle dissipated energy, $w = \int_{cycle} \boldsymbol{\sigma} : \dot{\boldsymbol{\varepsilon}}_m dt$, (Eq. 2). The stress ratio R_σ is defined as $R_\sigma = \sigma_{min}/\sigma_{max}$, where σ_{min} and σ_{max} are the minimal and the maximal principal stress over the loading cycle, respectively. The mean stress term for OP-TMF increases the modified dissipated energy per cycle. Therefore, the modified dissipated energy per cycle criterion predicts a shorter lifetime in the OP-TMF tests, assuming positive parameter α. The criterion presented here predicts a longer lifetime for cases, where negative mean stress is present, as in the case of IP-TMF.

Table 3: Damage model parameters.

Criterion	A	B	α	R^2
w	87.096	-0.624	-	0.740
$\widetilde{w}$	87.096	-0.624	4.239	0.882

The model parameters and the corresponding coefficient of determination are presented in Tab. 3 [A.1], where results are also presented for a criterion with no additional terms corresponding to the classical dissipated energy per cycle criterion, i.e. $\widetilde{w} = w$, this criterion doesn't render the role of the mean stress. If we compare the obtained R^2, one can note that the modified dissipated energy per cycle fits the OP-TMF experimental results better. The predicted number of cycles to failure versus the observed number of cycles to failure is plotted in Fig. 16b [A.1] for the modified dissipated energy per cycle criterion, and in Fig. 16a for the dissipated energy per cycle criterion [A.1]. The 95% prediction interval (dashed lines) almost coincides with a two times band for the proposed model. This indicates a reliable fatigue predictions. In conclusion, simplicity and robustness is characteristic for the proposed criterion. The criterion can

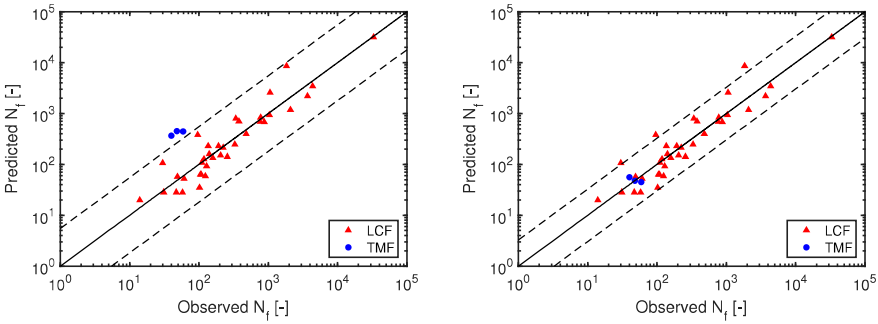

(a) (b)

Figure 16: Dissipated energy per cycle criterion (a) and modified dissipated energy per cycle criterion (b). Observed and predicted lifetime for specimens.

be implemented as a post-processing program for finite-element software [A.6, A.17, A.18].

8 Outcomes

8.1 Theoretical outcomes

High temperature data LCF and TMF data are mostly not published in its raw form and therefore may not be reused. The presented experimental data for SiMo 4.06 in this work have been published in its raw form in [A.1, A.3]. This can be used in order to study material models and damage models without the need to obtain own original experimental data. The implementation of a unified viscoplastic model in the framework of finite element method and consistent tangent stiffness was published in [A.3]. This will allow another researchers to speed up the development of their own modifications of material models, especially the derivation of consistent tangent stiffness. The proposed energy based fatigue criterion can be used for fatigue predictions under LCF and TMF loading conditions. The criterion can be further studied and modified if needed. The proposed criterion is alternative to complicated phenomenological lifetime prediction models. The criterion is suitable to be used for the unified viscoplastic material models.

8.2 Practical outcomes

The introduced newly in-house designed test can be used for performing LCF and TMF uniaxial tests on specimens. The obtained results can be used in or-

der to calibrate most commonly used engineering material models [A.2, A.10]. The selected unified viscoplastic material model is implemented as UMAT for Abaqus, so that it can be used for solving practical problems. The material model can be used for simulation of mechanical response under the complex anisothermal loading conditions. The formulated consistent tangent stiffness is a key point for solving large-scale engineering problems. The proposed energy based fatigue criterion can be used for fatigue analysis with the advantage of low numerical costs in comparison with the methods assuming critical plane approach. The calibration of the criterion does not require expensive test stands, such as those with climatic chamber. The presented results may be used for damage assessment method of complex engineering components that are subjected to high temperature LCF and TMF loading.

9 Conclusions and future work

9.1 Conclusions

The aims of the thesis were accomplished with the following comments:

1. A novel energy based fatigue criterion was proposed in order to predict LCF/TMF lifetime for specimens and for complex engineering structures. A reasonable correlation was achieved between the observed results and the predicted results. The proposed fatigue criterion was published in [A.1]. The development of the criterion was published in [A.11].

2. The proposed control and control algorithms for the new in-house designed test stand enable strain-controlled high temperature uniaxial LCF and TMF tests performed on specimens. The results were given in Chapter 5 and published in [A.1, A.9, A.12].

3. Large amount of new experimental data was generated for SiMo for temperatures between 20°C and 750°C. This can be used for calibration of constitutive material models and for fatigue analysis. The experimental results presented here were published in [A.1], [A.9]-[A.15]. Experimental data were also published together with computations in [A.2]-[A.12].

4. A unified viscoplastic material model was implemented as UMAT for Abaqus. The consistent tangent stiffness was derived on the basis of numerical integration scheme, and verified on the numerical example. The results were described in Chapter 6. The implementation of material model and its calibration were published in [A.3, A.5].

5. The temperature dependent unified viscoplastic material model was calibrated from the obtained experimental data. The non-linear kinematic hardening model parameters were calibrated systematically with temperature, mathematically represented as a Boltzmann function. A reasonable correlation was achieved between the observed results and the predicted results. The calibration of the viscoplastic model was published in [A.3, A.5]. The calibration of temperature dependent kinematic hardening parameters was also included in [A.2, A.4, A.7, A.8, A.10]. The systematically calibrated temperature dependent kinematic hardening parameters were used for a engineering failure analysis of a turbine housing in [A.2].

9.2 Future work and outlook

Possible topics for future research for SiMo 4.06 are IP-TMF tests and LCF tests with long dwell times. Verification of the fatigue proposed criterion should be done in terms of IP-TMF tests. Next, longer dwell times during the LCF or TMF may introduce additional cyclic softening. The possible need of modifications may arise, for the used unified material model and for the proposed fatigue criterion. Furthermore, the mechanical behaviour of metal materials subject to proportional, and in particular non-proportional, multiaxial thermo-mechanical loading is generally a subject of future interest and research. This covers validation of commonly used constitutive material models and as well as validation of commonly used damage models. However, this will require multiaxial thermo-mechanical fatigue test stands, which are very expensive in general.

References

[1] Amiable, S., Chapuliot, S., Constantinescu, A., and Fissolo, A. A computational lifetime prediction of a thermal shock experiment. part i: thermomechanical modelling and lifetime prediction. *Fatigue & Fracture of Engineering Materials & Structures 29*, 3 (2006), 175–182.

[2] Amiable, S., Chapuliot, S., Constantinescu, A., and Fissolo, A. A computational lifetime prediction of a thermal shock experiment. part ii: discussion on difference fatigue criteria. *Fatigue & Fracture of Engineering Materials & Structures 29*, 3 (2006), 219–227.

[3] Armstrong, P. J., and Frederick, C. *A mathematical representation of the multiaxial Bauschinger effect*, vol. 731. Central Electricity Generating Board [and] Berkeley Nuclear Laboratories, Research & Development Department Berkeley, 1966.

[4] Barrett, R., Farragher, T., Hyde, C. J., O'Dowd, N., O'Donoghue, P., and Leen, S. B. A unified viscoplastic model for high temperature low cycle fatigue of service-aged p91 steel. *Journal of Pressure Vessel Technology 136*, 2 (2014), 021402.

[5] Barrett, R. A., O'Donoghue, P., and Leen, S. B. An improved unified viscoplastic constitutive model for strain-rate sensitivity in high temperature fatigue. *International Journal of Fatigue 48* (2013), 192–204.

[6] Beck, T., Pitz, G., Lang, K.-H., and Löhe, D. Thermal-mechanical and isothermal fatigue of in 792 cc. *Materials Science and Engineering: A 234* (1997), 719–722.

[7] Beck, T., and Rau, K. Temperature measurement and control methods in tmf testing–a comparison and evaluation. *International journal of fatigue 30*, 2 (2008), 226–233.

[8] Bodner, S., and Partom, Y. Constitutive equations for elastic-viscoplastic strain-hardening materials. *Journal of Applied Mechanics 42*, 2 (1975), 385–389.

[9] Cailletaud, G., and Sai, K. Study of plastic/viscoplastic models with various inelastic mechanisms. *International Journal of Plasticity 11*, 8 (1995), 991–1005.

[10] Chaboche, J.-L. Time-independent constitutive theories for cyclic plasticity. *International Journal of plasticity 2*, 2 (1986), 149–188.

[11] Chaboche, J.-L. Constitutive equations for cyclic plasticity and cyclic viscoplasticity. *International journal of plasticity 5*, 3 (1989), 247–302.

[12] Chaboche, J.-L. A review of some plasticity and viscoplasticity constitutive theories. *International journal of plasticity 24*, 10 (2008), 1642–1693.

[13] Coffin Jr, L. F. A study of the effects of cyclic thermal stresses on a ductile metal. *Transactions of the American Society of Mechanical Engineers, New York 76* (1954), 931–950.

[14] Constantinescu, A., Charkaluk, E., Lederer, G., and Verger, L. A computational approach to thermomechanical fatigue. *International Journal of fatigue 26*, 8 (2004), 805–818.

[15] Contesti, E., and Cailletaud, G. Description of creep-plasticity interaction with non-unified constitutive equations: application to an austenitic stainless steel. *Nuclear engineering and design 116*, 3 (1989), 265–280.

[16] Dunne, F., and Petrinic, N. *Introduction to computational plasticity.* Oxford University Press on Demand, 2005.

[17] Hähner, P., Affeldt, E., Beck, T., Klingelhöffer, H., Loveday, M., and Rinaldi, C. Validated code-of-practice for strain-controlled thermo-mechanical fatigue testing. *Institute for Energy, Petten* (2006).

[18] Hähner, P., Rinaldi, C., Bicego, V., Affeldt, E., Brendel, T., Andersson, H., Beck, T., Klingelhöffer, H., Kühn, H.-J., Köster, A., et al. Research and development into a european code-of-practice for strain-controlled thermo-mechanical fatigue testing. *International Journal of Fatigue 30*, 2 (2008), 372–381.

[19] Halford, G., and Manson, S. Life prediction of thermal-mechanical fatigue using strainrange partitioning. In *Thermal fatigue of materials and components*. ASTM International, 1976.

[20] Hebák, P., Hustopeckỳ, J., and Malá, I. *Vícerozměrné statistické metody 2.* Informatorium, 2005.

[21] Heitmann, H., Vehoff, H., and Neumann, P. Life prediction for random load fatigue based on the growth behavior of microcracks. In *Fracture 84*. Elsevier, 1984, pp. 3599–3606.

[22] Hosseini, E., Holdsworth, S., Kühn, I., and Mazza, E. Temperature dependent representation for chaboche kinematic hardening model. *Materials at High Temperatures 32*, 4 (2015), 404–412.

[23] Kawai, M., and Ohashi, Y. Couple effect between creep and plasticity of type 316 stainless steel at elevated temperature. Tech. rep., Los Alamos National Lab., NM (USA); Nagoya Univ.(Japan); Aichi Inst. of Tech ..., 1987.

[24] Kichenin, J. *Comportement Thermomecanique du Polyethylene—Application aux Structures Gazieres.* PhD thesis, Ecole Polytechnique, Palaiseau, France, 1995.

[25] Kullig, E., and Wippler, S. Numerical integration and fem-implementation of a viscoplastic chaboche-model with static recovery. *Computational Mechanics 38*, 6 (2006), 1–13.

[26] Lemaitre, J., and Chaboche, J.-L. *Mechanics of solid materials.* Cambridge university press, 1994.

[27] Manson, S. S. Behavior of materials under conditions of thermal stress.

[28] MATLAB. *MATLAB R2018b Documentation.* The MathWorks Inc., Natick, Massachusetts, 2018.

[29] Miller, A. An inelastic constitutive model for monotonic, cyclic, and creep deformation: Part i—equations development and analytical procedures. *Journal of Engineering Materials and Technology 98*, 2 (1976), 97–105.

[30] Moré, J. J., and Sorensen, D. C. Computing a trust region step. *SIAM Journal on Scientific and Statistical Computing 4*, 3 (1983), 553–572.

[31] Murakami, S., and Ohno, N. A constitutive equation of creep based on the concept of a creep-hardening surface. *International Journal of Solids and Structures 18*, 7 (1982), 597–609.

[32] Nagode, M. Continuous damage parameter calculation under thermo-mechanical random loading. *MethodsX 1* (2014), 81–89.

[33] Nagode, M., Hack, M., and Fajdiga, M. Low cycle thermo-mechanical fatigue: damage operator approach. *Fatigue & Fracture of Engineering Materials & Structures 33*, 3 (2010), 149–160.

[34] Nagode, M., Längler, F., and Hack, M. A time-dependent damage operator approach to thermo-mechanical fatigue of ni-resist d-5s. *International Journal of Fatigue 33*, 5 (2011), 692–699.

[35] Neu, R., and Sehitoglu, H. Thermomechanical fatigue, oxidation, and creep: Part i. damage mechanisms. *Metallurgical and Materials Transactions A 20*, 9 (1989), 1755–1767.

[36] Neu, R., and Sehitoglu, H. Thermomechanical fatigue, oxidation, and creep: Part ii. life prediction. *Metallurgical Transactions A 20*, 9 (1989), 1769–1783.

[37] Norman, V., Skoglund, P., Leidermark, D., and Moverare, J. Damage mechanisms in silicon-molybdenum cast irons subjected to thermo-mechanical fatigue. *International Journal of Fatigue 99* (2017), 258–265.

[38] Ostergren, W. A damage function and associated failure equations for predicting hold time and frequency effects in elevated temperature, low cycle fatigue. *Journal of Testing and Evaluation 4*, 5 (1976), 327–339.

[39] Petráš, R., Škorík, V., and Polák, J. Thermomechanical fatigue and damage mechanisms in sanicro 25 steel. *Materials Science and Engineering: A 650* (2016), 52–62.

[40] Prager, W. Recent developments in the mathematical theory of plasticity. *Journal of applied physics 20*, 3 (1949), 235–241.

[41] Sehitoglu, H. Thermo-mechanical fatigue life prediction methods. In *Advances in fatigue lifetime predictive techniques*. ASTM International, 1992.

[42] Simo, J. C., and Hughes, T. J. *Computational inelasticity*, vol. 7. Springer Science & Business Media, 2006.

[43] Simo, J. C., and Taylor, R. L. Consistent tangent operators for rate-independent elastoplasticity. *Computer methods in applied mechanics and engineering 48*, 1 (1985), 101–118.

[44] Smith, K. N. A stress-strain function for the fatigue of metals. *Journal of materials 5* (1970), 767–778.

[45] Tabibian, S., Charkaluk, E., Constantinescu, A., Szmytka, F., and Oudin, A. Tmf–lcf life assessment of a lost foam casting a319 aluminum alloy. *International Journal of Fatigue 53* (2013), 75–81.

[46] Taira, S. Relationship between thermal fatigue and low-cycle fatigue at elevated temperature. In *Fatigue at elevated temperatures*. ASTM International, 1973.

[47] Wu, X., Quan, G., MacNeil, R., Zhang, Z., Liu, X., and Sloss, C. Thermomechanical fatigue of ductile cast iron and its life prediction. *Metallurgical and Materials Transactions A 46*, 6 (2015), 2530–2543.

Publications related to the title of Dissertation

Reviewed papers

[A.1] Bartošák, M., Novotný, C., Španiel, M., Doubrava K. Life assessment of SiMo 4.06 cast iron under LCF and TMF loading conditions. *Materials at High Temperatures* (2018), DOI 10.1080/09603409.2018.1542825.

[A.2] Bartošák, M., Španiel, M., Doubrava K. Thermo-Mechanical Fatigue of SiMo 4.06 Turbocharger Turbine Housing: Damage Operator Approach. Under review in journal *Engineering Failure Analysis.*

[A.3] Bartošák, M., Španiel, M., Doubrava K. FEM Implementation of a unified viscoplastic model and its application to modelling cyclic mechanical behaviour of ductile cast iron under LCF and TMF loading conditions. Under review in journal *Materials at High Temperatures.*

Conference contributions

[A.4] Bartošák, M., Španiel, M., Černý, J. Lifetime calculation for turbine housing of turbocharger under thermo-mechanical loading: damage operator approach. In: *LCF 8, Eighth International Conference on Low Cycle Fatigue*, Dresden: The German Association for Materials Research and Testing, 2017, 93–98. ISBN 978-3-9814516-5-8.

[A.5] Bartošák, M., Španiel, M. Implementation of Unified Viscoplastic Chaboche Model. In: *33rd conference with international participation Computational Mechanics 2017 - Extended Abstracts*, Pilsen: University of West Bohemia, 2017, 5–6. ISBN 978-80-261-0748-4.

[A.6] Bartošák, M., Španiel, M. POST-PROCESSING PROGRAM FOR THERMO-MECHANICAL FATIGUE. In: *21st Workshop of Applied Mechanics - Proceedings*, Praha: České vysoké učení technické v Praze, Fakulta strojní, 2016, 5–8. ISBN 978-80-01-06085-8.

[A.7] Bartošák, M. LIFETIME CALCULATION FOR TURBINE HOUSING OF TURBOCHARGER UNDER THERMOMECHANICAL LOADING. In: *20th Workshop of Applied Mechanics - Book of Papers*, Praha: České vysoké učení technické v Praze, Fakulta strojní, 2016. ISBN 978-80-01-05975-3.

[A.8] Bartošák, M., Španiel, M. Thermomechanical Fatigue and Creep of Turbine Housing of Turbocharger: Damage Operator Approach. In: *Studentská tvůrčí činnost 2016*, Praha: České vysoké učení technické v Praze, Fakulta strojní, 2016. ISBN 978-80-01-05929-6.

[A.9] Bartošák, M., Španiel, M., Doubrava K., Novotný, C. Isothermal LCF,

relaxation and thermomechanical fatigue tests of Si-Mo based cast iron. In: *Experimental Stress Analysis 2016*, Plzeň: Západočeská universita, Fakulta aplikovaných věd, 2016. ISBN 978-80-261-0624-1.

[A.10] Bartošák, M., Španiel, M., Nesládek M. THERMO-MECHANICAL FATIGUE OF SI-MO 4.06 TURBINE HOUSING OF TURBOCHARGER - DAMAGE OPERATOR BASED LIFETIME PREDICTIONS. In: *Engineering Mechanics 2016 - Book of full texts*, Prague: Institute of Thermomechanics, AS CR, v.v.i., 2016, 46–49. ISSN 1805-8248. ISBN 978-80-87012-59-8.

[A.11] Bartošák, M. LOW-CYCLE THERMO-MECHANICAL FATIGUE OF DUCTILE CAST IRON. In: *Workshop of Applied Mechanics 2015 (19-th WAM)*, Praha: České vysoké učení technické v Praze, Fakulta strojní, 2015.

[A.12] Bartošák, M. THERMOMECHANICAL FATIGUE EXPERIMENTS. In: *18th Workshop of Applied Mechanics*, Praha: České vysoké učení technické v Praze, Fakulta strojní, 2015. ISBN 978-80-01-05746-9.

Research reports

[A.13] Španiel, M., Bartošák, M. *Experimentální stanovení Manson-Coffinovy křivky materiálu skříní turbodmychadel.* [Research report]. Praha: ČVUT v Praze, FS, 2014. 12105/2014/27. [in Czech].

[A.14] Bartošák, M., Španiel, M. *Material model for assessment of low-cycle thermo-mechanical fatigue.* [Research report]. Praha: ČVUT FS, Ústav mechaniky, Odbor pružnosti a pevnosti, 2015. 12105/15/25.

[A.15] Bartošák, M., Španiel, M. *Implementation of material model for low-cycle thermo-mechanical fatigue.* [Research report]. Praha: ČVUT FS, Ústav mechaniky, Odbor pružnosti a pevnosti, 2016. 12105/16/27.

Functional specimens

[A.16] Španiel, M., Novotný, C., Bartošák, M. *Přípravek pro zkoušky teplotně-mechanické únavy dle Coffina.* [Functional specimen]. 2013.

Software

[A.17] Bartošák, M., Španiel, M. *Software routines for material model of low-cycle thermo-mechanical fatigue in Abaqus FEM software.* [Software]. 2016.

[A.18] Bartošák, M., Španiel, M. *Software routines for material model of low-cycle thermo-mechanical fatigue in Abaqus FEM software. Visco-plastic approximation.* [Software]. 2017.